Partial and split dislocation configurations in nanocrystalline metals

S. V. Bobylev, M. Yu. Gutkin, and I. A. Ovid'ko*
Institute of Problems of Mechanical Engineering, Russian Academy of Sciences, Bolshoj 61, Vas. Ostrov, St. Petersburg 199178, Russia
(Received 31 October 2005; published 3 February 2006)

A theoretical model is suggested that describes the generation of partial and split dislocations at grain boundaries in nanocrystalline metals. The ranges of parameters (such as grain size and level of external stress) are theoretically revealed at which the formation of partial dislocation semi-loops is energetically favorable. It is shown that anomalously wide stacking faults between partial dislocations—elements of split dislocations—are formed due to the effects of high stresses existing in nanocrystalline metals under mechanical load. The results of the suggested model account for experimental data on observation of partial and split dislocation configurations in nanocrystalline Al reported in the literature.

DOI: 10.1103/PhysRevB.73.064102 PACS number(s): 62.25.+g, 61.46.−w

I. INTRODUCTION

Defects in solid state nanostructures often crucially affect their outstanding physical and mechanical properties and thereby represent the subject of rapidly growing fundamental and applied research efforts. In doing so, partial and split dislocations are recognized as typical defects in solid state nanostructures such as nanocrystalline metals,[1–12] semiconductor quantum dots,[13–17] nanoscale films,[18–21] and nanostructured grain boundaries (GBs) in high-transition-temperature superconductors[22–26] and perovskite oxide $SrTiO_3$.[27] As shown by experimental study, computer simulations, and theoretical analysis,[1–27] the formation of these dislocation configurations in solid state nanostructures is enhanced due to the interface and nanoscale effects. At the same time, partial and split dislocation configurations are capable of strongly influencing functional and structural properties of nanostructures. In particular, plastic deformation mode carried by partial and split dislocation configurations is among specific physical mechanisms of plastic deformation in nanocrystalline solids[1–12,28–31] whose mechanical properties commonly are enhanced compared to those of their coarse-grained counterparts. The conventional lattice dislocation slip is suppressed by GBs in nanocrystalline metals with finest grains (having the mean grain size lower than a critical value of around 20–30 nm), in which volume fractions of GBs and their triple junctions are extremely large. In nanocrystalline solids with the finest grains, the GBs and their triple junctions come into play as new sources and channels of plasticity. Pure nanocrystalline Al is a good example to demonstrate the unusual mechanisms of plastic deformation in nanocrystalline metals. Molecular dynamics simulations[2,11,12] have shown that plastic deformation of nanocrystalline Al with very small grains (from 5 to 10 nm) is realized through intergrain sliding and grain rotation. When the grain size achieves some tens of nanometers, the generation of partial and split dislocations by GBs dominates over the other mechanisms.[12,32–34] Partial dislocations, wide strips of stacking faults, and deformation twins in pure nanocrystalline Al were observed in transmission electron microscopy (TEM) and high-resolution TEM (HRTEM) experiments.[6–9] The stacking fault (SF) strips between partial dislocations in nanocrystalline Al occurred to be 1.5–11 times wider than in conventional coarse-grained Al.[9] This observation is in conflict with the traditional view that dislocation splitting and deformation twinning are practically impossible in pure Al due to its high SF energy.[35]

To understand the reasons for dislocation splitting and abnormal widening of SFs in pure nanocrystalline Al, several theoretical models have been proposed,[9,36–39] describing the energy characteristics of emission of partial dislocation semiloops from GBs. The general issue is that the small grain size is directly responsible for these phenomena. Following the models,[9,36–39] the SF strips must become wider when the grain size drops. This important result seems to be weakly proved due to some common lacks of these models. First, the energy calculations were rather rough because they used the solution for the strain energy of a straight infinite dislocation to approximate the self-energies of finite dislocation segments composing the partial dislocation semiloops, and neglected the interaction energy terms. Second, it was assumed that one partial dislocation semiloop remains immobile when the other expands. Third, the real geometry of partial dislocation semiloop glide was not taken into account. As shown in our theoretical analysis in this paper, the approaches[9,36–38] give no reliable results.

The main aim of this paper is to suggest a three-dimensional (3D) theoretical model describing the emission of partial dislocation semiloops from GBs in nanocrystalline metals. This model is based on strict calculations of energies of elastically interacting dislocation loops taking into account the real geometry of their glide in the exemplary case of nanocrystalline Al. We show that the grain size does not influence directly the width of dislocation splitting. It is the high level of applied elastic stress that plays the crucial role, and the small grain size just provides a possibility to achieve this level in a nanocrystalline metal.

II. INTERGRAIN SLIDING IN NANOCRYSTALLINE SOLIDS: GENERAL ASPECTS

Following Refs. 2–5, 12, and 27–30, intergrain sliding essentially contributes to plastic flow in nanocrystalline metals with the finest grains. The intergrain sliding in high-angle GBs in coarse-grained and nanocrystalline solids occurs by

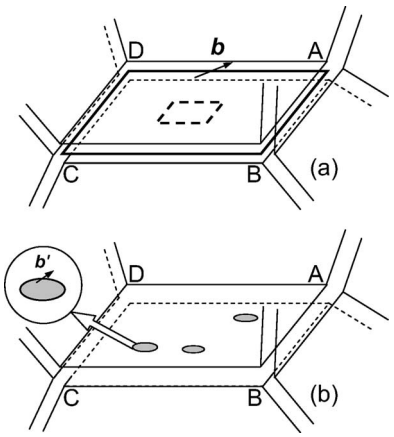

FIG. 1. Intergrain sliding mechanisms. (a) Expansion of a gliding GB dislocation loop with the Burgers vector $\boldsymbol{b}$ in GB ABCD conducts intergrain sliding localized at the dislocation core. The dislocation loop in its initial and final state is shown as dashed and solid rectangle, respectively. (b) Uncorrelated local shear events in free-volume defects (gray spheroids) in a GB ABCD conduct homogeneous intergrain sliding. Each uncorrelated local shear event is equivalent to the generation of a nanoscale dislocation loop as shown in the magnified inset.

either uncorrelated local shear events or movement of GB dislocations (Fig. 1).[3,40,41]

In particular, the intergrain sliding in coarse-grained and nanocrystalline solids can be effectively conducted by movement of gliding GB dislocations with Burgers vectors parallel with corresponding GB planes [Fig. 1(a)].[40] Such GB dislocations with ordered structures are defined as defects violating translation symmetries of GBs. They are characterized by Burgers vectors whose magnitudes are small (each magnitude ranges from tentatively $a/5$ to $a/3$) and defined by translational symmetries of the GB structures.[40] Glide of GB dislocations with Burgers vectors parallel with corresponding GB planes is driven by the shear stress and conducts intergrain sliding localized in the dislocation core. For illustration, expansion of a gliding GB dislocation loop under the shear stress action is shown in Fig. 1(a).

The triple junction of GBs serve as borders between the GB and bulk (grain interior) phases. Therefore the triple junctions represent geometric obstacles for the glide of GB dislocations from a GB towards the adjacent grain interiors. In these circumstances, expansion of gliding GB dislocation loops in a GB is restricted by the triple junctions, borders of the GB area [Fig. 1(a)]. At certain conditions, further evolution of such GB dislocation loops can occur through emission of semiloops of partial dislocations into adjacent grain interiors. A theoretical analysis of the emission of partial dislocations from dislocated GBs will be done in the next section.

Besides the dislocation theory[40] of intergrain sliding, there is an alternative view[3,40,41] that intergrain sliding in GBs in nanocrystalline solids is carried by free-volume defects, nanometer-size spheroidal regions where the shear resistance is less than in the rest of the GB due to the presence of an extra free volume [Fig. 1(b)]. Ensembles of such free-volume defects homogeneously distributed in the GB phase provide

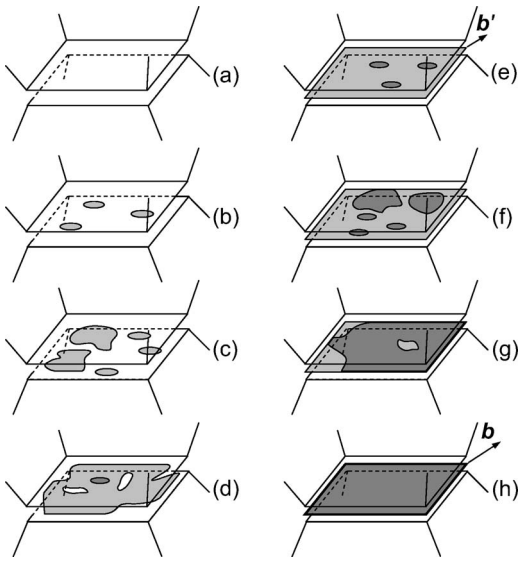

FIG. 2. Intergrain sliding through uncorrelated events of the nanoscale dislocation loop generation (local shear events in free-volume defects) in a GB results in the formation of a defect similar to the GB dislocation loop with a large Burgers vector. (a) GB in its initial state is free from any dislocationlike defects. (b) Several nanoscale dislocation loops (gray ellipses) are generated in GB under the shear stress action. (c) New nanoscale dislocation loops are generated in GB. Also, several nanoscale dislocation loops converge, thus forming a dislocation loop of intermediate size. (d) Most nanoscale dislocation loops converge forming a continuous large dislocation loop having the Burgers vector $\boldsymbol{b}'$ and occupying the GB area as a whole. (e) New nanoscale dislocation loops (dark ellipses) are generated in the GB region swept by the previously formed large dislocation loop (gray region). (f) Several newly generated nanoscale dislocation loops converge and form a dislocation loop (dark region) of intermediate size. (g) Most nanoscale dislocation loops converge forming a continuous large dislocation loop having the Burgers vector $\boldsymbol{b}$ and occupying the GB area as a whole.

uncorrelated local shear events as elementary acts of intergrain sliding.[3,40,41] These shear events are driven by the shear stress and carry homogeneous intergrain sliding in GBs, especially in GBs having a nonequilibrium, disordered structure. The discussed view is based on the concept[42] of free-volume defects providing local shear events as elemental acts of homogeneous plastic deformation in amorphous materials. In this context, with the interpretation[42] of local shear events as events of the generation of nanoscale dislocation loops, one finds that the intergrain sliding by local shear events can produce GB defects which are very similar to the conventional GB dislocation loop. Actually, since triple junctions serve as obstacles for intergrain sliding, numerous local shear events, occurring in a GB, result in the accumulation of the unfinished shear or, in other words, dislocation charge at the borders of the GB area (Fig. 2). As a corollary, numerous local shear events, occurring in a GB, form a rectangular dislocation loop (Fig. 2) which looks like a conventional GB dislocation loop shown in Fig. 1(a). The difference between the dislocation loop [Fig. 2(h)] and the conventional GB dislocation loop is in the magnitude of their Burgers vectors. The conventional GB dislocation loops are characterized by

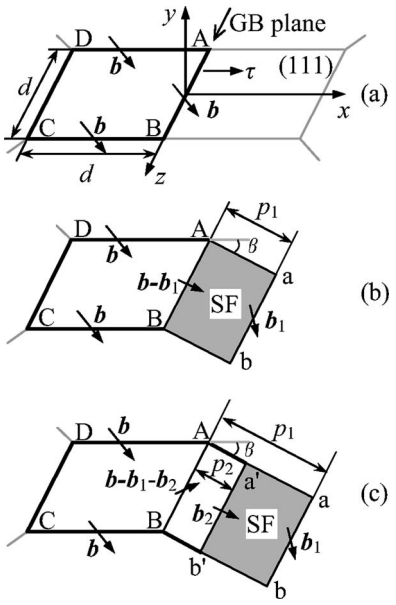

FIG. 3. A schematic illustration of the generation of the partial dislocation loops with Burgers vectors $\boldsymbol{b}_1$ and $\boldsymbol{b}_2$ at the preexistent GB dislocation loop ABCD with Burgers vector $\boldsymbol{b}$.

Burgers vectors whose magnitudes are small (each magnitude ranges from tentatively $a/5$ to $a/3$) and defined by translational symmetries of the ordered GB structures.[40] The dislocation loop [Fig. 2(h)] resulted from numerous local shear events in a disordered GB is characterized by a Burgers vector whose magnitude is arbitrary. Generally speaking, since the dislocation loop [Fig. 2(h)] represents a superposition of numerous nanoscale dislocation loops [associated with local shear events (Fig. 2)], it should be considered as a loop of Somigliana dislocation having a variable Burgers vector. However, for simplicity of our further theoretical analysis of emission of partial dislocations from GBs, we suppose the dislocation loop [Fig. 2(h)] to be a GB (Volterra) dislocation loop with a constant Burgers vector of arbitrary magnitude (say, ranging from $a/5$ to $3a$).

The aforesaid allows us to treat the GB dislocation loops at GBs as typical GB defects resulting from intergrain sliding conducted by either local shear events or conventional GB dislocations. The Burgers vector magnitudes of GB dislocation loops [Fig. 2(h)] resulted from numerous local shear events can be comparatively large (say, exceed the crystal lattice parameter a).

III. EMISSION OF PARTIAL DISLOCATION SEMILOOPS FROM DISLOCATED GB: MODEL

Now let us consider a model of the emission of partial dislocation semiloops from a GB containing a GB dislocation loop in a fcc metal. The system in its initial state is represented by a dislocation loop ABCD with the Burgers vector $\boldsymbol{b}$ (hereinafter called $\boldsymbol{b}$-loop) formed within the GB [Fig. 3(a)]. For simplicity, both the grain and loop are assumed to have square shape and size d. Under an applied shear stress τ two partial dislocation semiloops (AabB and Aa′b′B) with the Burgers vectors $\boldsymbol{b}_1$ and $\boldsymbol{b}_2$ are formed one after another at the $\boldsymbol{b}$-loop segment AB [Figs. 3(b) and 3(c)]. The shaded area a′abb′ in Figs. 3(b) and 3(c) denotes the SF between the partial dislocation semiloops. The combination of the Burgers vectors $\boldsymbol{b}_1$ and $\boldsymbol{b}_2$ with the gliding plane defines the gliding system. Following Zhu *et al.*,[37,38] we consider two gliding systems called the 60°-I system and the screw system comprised of the following dislocations: dislocations with the Burgers vectors $\boldsymbol{b}_1=a/6[11\bar{2}]$ and $\boldsymbol{b}_2=a/6[2\bar{1}\bar{1}]$, for the 60°-I system; and dislocations with the Burgers vectors $\boldsymbol{b}_2=a/6[1\bar{2}1]$ and $\boldsymbol{b}_1=a/6[2\bar{1}\bar{1}]$, for the screw system. Here a is the lattice parameter. The gliding plane is (111) in both systems, and the GB, at which the partial dislocation semiloops are generated, is oriented along $[1\bar{1}0]$. The sum of the Burgers vectors $\boldsymbol{b}_1$ and $\boldsymbol{b}_2$ gives the lattice Burgers vector $\boldsymbol{b}_0$, in which case $\boldsymbol{b}_0=a/2[10\bar{1}]$, for the 60°-I system, and $\boldsymbol{b}_0=a/2[1\bar{1}0]$, for the screw system.

Under an applied stress τ, the partial dislocation semiloops expand by the glide of segments ab and a′b′. The other segments of the $\boldsymbol{b}$-loop are assumed to be immobile. To analyze the generation and expansion of the partial dislocation semiloops, let us calculate the corresponding changes in the total energy of the system.

The total energy of the system in its initial state [Fig. 3(a)] is $W_0=W_s+W_c$, where W_s and W_c are the strain and core energies, respectively, of the $\boldsymbol{b}$-loop. After emission of the first partial dislocation semiloop [Fig. 3(b)], the system may be decomposed into two dislocation loops: the initial $\boldsymbol{b}$-loop and a new rectangular loop of partial dislocation with the Burgers vector $\boldsymbol{b}_1$ ($\boldsymbol{b}_1$-loop). The energy W_1 of such a dislocation configuration depends on the path p_1 moved by the gliding dislocation segment ab:

$$W_1(p_1) = W_s + W_{s1}(p_1) + W_{int1}(p_1) + W_c' + W_{c1}'(p_1) + W_{c0} + W_{f1}(p_1), \tag{1}$$

where $W_{s1}(p_1)$ is the self-strain energy of the $\boldsymbol{b}_1$-loop, $W_{int1}(p_1)$ the energy of elastic interaction between the $\boldsymbol{b}$- and $\boldsymbol{b}_1$-loops, W_c' the sum core energy of the three segments of the $\boldsymbol{b}$-loop that stay unchanged during generation of the $\boldsymbol{b}_1$-loop, $W_{c1}'(p_1)$ the sum core energy of the dislocation segments Aa, ab, and Bb of the $\boldsymbol{b}_1$-loop, W_{c0} the core energy of the segment AB belonging to both the $\boldsymbol{b}$- and $\boldsymbol{b}_1$-loops, and $W_{f1}(p_1)=\gamma(d-2b_1)(p_1-r_{c1}-r_{c2})$ the energy of SF in the region AabB. Here γ is the specific SF energy and r_{ci} is the core radius of the segments ab($i=1$) and AB ($i=2$).

Similarly, after emission of the second partial dislocation semiloop [Fig. 3(c)], the system may be decomposed into three dislocation loops: the $\boldsymbol{b}$- and $\boldsymbol{b}_1$-loops, and a new rectangular loop of partial dislocation with the Burgers vector $\boldsymbol{b}_2$ ($\boldsymbol{b}_2$-loop). The corresponding total energy W_2 depends on two paths p_1 and p_2 moved by the segments ab and a′b′, respectively:

$$W_2(p_1,p_2) = W_s + W_{s1}(p_1) + W_{s2}(p_2) + W_{int1}(p_1) + W_{int2}(p_2) + W_{int3}(p_1,p_2) + W_c' + W_{c1}''(p_1,p_2) + W_{c2} + W_{c3}(p_2) + W_{c0}' + W_{f2}(p_1,p_2), \quad (2)$$

where $W_{s2}(p_2)$ is the self-strain energy of the $\boldsymbol{b}_2$-loop, $W_{int2}(p_2)$ the energy of elastic interaction of the $\boldsymbol{b}$- and $\boldsymbol{b}_2$-loops, $W_{int3}(p_1,p_2)$ the energy of elastic interaction of the $\boldsymbol{b}_1$- and $\boldsymbol{b}_2$-loops, $W_{c1}''(p_1)$ the sum core energy of the dislocation segments a′a, ab, and bb′, W_{c2} the core energy of the segment a′b′, $W_{c3}(p_2)$ the sum core energy of the segments Aa' and Bb′ formed due to overlapping of the $\boldsymbol{b}_1$- and $\boldsymbol{b}_2$-loops, W_{c0}' the core energy of the segment AB belonging to the $\boldsymbol{b}$-, $\boldsymbol{b}_1$-, and $\boldsymbol{b}_2$-loops, and $W_{f2}(p_1,p_2)=\gamma(d-2b_1)(p_1-p_2-r_{c1}-r_{c2})$ the SF energy in the region a′abb′.

Following Ref. 43, the self-energies $W_{si}(p_i)$ read

$$W_{si}(p_i) = Db_i^2\left\{(2-\nu)(h_i-p_i-d) + (1-\nu\sin^2\alpha_i)d\ln\frac{2p_id}{r_{ci}(h_i+d)} + (1-\nu\cos^2\alpha_i)p_i\ln\frac{2p_id}{r_{ci}(h_i+p_i)}\right\}, \quad (3)$$

where $D=G/[2\pi(1-\nu)]$, G is the shear modulus, ν is the Poisson ratio, $h_i^2=p_i^2+d^2$, and α_i is the angle between the Burgers vector $\boldsymbol{b}_i$ and axis x. The interaction energies can be found as the work spent to generate one dislocation loop in the stress field of the other.[44] Using the elastic stress fields found in Ref. 45, we derive:

$$W_{int\,i}(p_i) = \frac{Dbb_i}{2}\left\{\cos\alpha\cos\alpha_i\left[\cos\beta\sqrt{X^2+u^2} + x_1x'\sin\beta\frac{\sqrt{X^2+u^2}}{X^2} - x'[\sin^2 2\beta-(1-\nu)\cos 2\beta]\ln(v+\sqrt{X^2+u^2})\right.\right.$$
$$-\frac{\cos\beta}{2|u|}(2x'^2\sin^2 2\beta-u^2)\ln\frac{\sqrt{X^2+u^2}-|u|}{\sqrt{X^2+u^2}+|u|} - \frac{x'^2\sin 4\beta\cos\beta}{|u|}\arctan\frac{|u|v}{x'\sin\beta\sqrt{X^2+u^2}}$$
$$+(1-\nu)\frac{\cos 2\beta}{2}\left[x_1\ln\frac{x_1^2\sin^2\beta+u^2}{(x_1\cos\beta-x'+\sqrt{X^2+u^2})^2}\right.$$
$$\left.\left.+\frac{2|u|}{\sin\beta}\left(\arctan\frac{|u|(v-\cos\beta\sqrt{X^2+u^2})}{\sin\beta[u^2+x'(x'-x_1\cos\beta+\sqrt{X^2+u^2})]}+\arctan\frac{|u|}{x_1\sin\beta}\right)\right]\right]$$
$$+\sin\alpha\sin\alpha_i\left[(2-\nu)\sqrt{X^2+u^2}+x'(\cos\beta\cos 2\beta+\sin^2\beta)\ln(v+\sqrt{X^2+u^2}) + (1-\nu)\frac{|u|}{2}\ln\frac{\sqrt{X^2+u^2}-|u|}{\sqrt{X^2+u^2}+|u|}\right.$$
$$\left.\left.+\frac{x_1\cos\beta}{2}\ln\frac{x_1^2\sin^2\beta+u^2}{(x_1\cos\beta-x'+\sqrt{X^2+u^2})^2}\right]\right\}\Bigg|_{x'=-d}^{x'=0}\Bigg|_{z'=-d/2}^{z'=d/2}\Bigg|_{x_1=r_c}^{x_1=p_i}\Bigg|_{z_1=-d/2}^{z_1=d/2}, \quad (4)$$

where $i=1,2$, α is the angle between the Burgers vector $\boldsymbol{b}$ and axis x, β is the angle between the planes of $\boldsymbol{b}$- and $\boldsymbol{b}_i$-loops, $X^2=x_1^2-2x_1x'\cos\beta+x'^2$, $u=z_1-z'$, $v=x_1-x'\cos\beta$, r_c the core radius of the $\boldsymbol{b}$-loop, and the notation $f(t)|_{t=p}^{t=q}=f(q)-f(p)$ is used. The energy of interaction between $\boldsymbol{b}_1$- and $\boldsymbol{b}_2$-loops is found in the same way as the formula above. It is given as follows:

$$W_{int3}(p_1,p_2) = -Db_1b_2\left\{(2-\nu)\cos(\alpha_1-\alpha_2)(h_1+h_2-S-d-2p_2) + d[\cos(\alpha_1-\alpha_2)-\nu\sin\alpha_1\sin\alpha_2]\times\ln\frac{2dp_1p_2(d+S)}{r_{c1}(p_1-p_2)(d+h_1)(d+h_2)}\right.$$
$$\left.+[\cos(\alpha_1-\alpha_2)-\nu\cos\alpha_1\cos\alpha_2]\times\left[p_1\ln\frac{p_1(p_1-p_2+S)}{(p_1-p_2)(p_1+h_1)} + p_2\ln\frac{4d^2(p_1-p_2)p_2}{r_{c1}^2(p_1-p_2+S)(p_2+h_2)}\right]\right\}. \quad (5)$$

Here $R_i^2=d^2+(d+p_i)^2$ and $S^2=d^2+(p_1-p_2)^2$. The core energies figuring on the right-hand side of formulas (1) and (2) are given by standard approximation which can be found elsewhere (e.g., see Ref. 46).

The evolution of the model system can be subdivided into four general acts which are (1) generation of the first partial dislocation semiloop accompanied by the energy change ΔW_1^g; (2) movement of the gliding dislocation segment ab of

the $\boldsymbol{b}_1$-loop [Fig. 3(b)], characterized by the energy change $\Delta W_1^m(p_1,\delta)$, where δ is a small displacement of the segment ab from its initial position p_1; (3) generation of the second partial dislocation semiloop accompanied by the energy change $\Delta W_2^g(p_1)$; and (4) combined movement of the segments ab and a′b′ of the $\boldsymbol{b}_1$- and $\boldsymbol{b}_2$-loops, respectively [Fig. 3(c)], characterized by the energy change $\Delta W_2^m(p_1, \delta_1, p_2, \delta_2)$, where δ_1 and δ_2 are some small displacements of the segments ab and a′b′from their initial positions p_1 and p_2, respectively. The total energy changes, characterizing these acts, can be expressed through the energies W_0, $W_1(p_1)$, and $W_2(p_1,p_2)$ given above as follows:

$$\Delta W_1^g = W_1(p_0) - W_0 - A_1(p_0), \tag{6}$$

$$\Delta W_1^m(p_1,\delta) = W_1(p_1+\delta) - W_1(p_1) - A_1(\delta), \tag{7}$$

$$\Delta W_2^g(p_1) = W_2(p_1,p_0) - W_1(p_1) - A_2(p_0), \tag{8}$$

$$\Delta W_2^m(p_1,\delta_1,p_2,\delta_2) = W_2(p_1+\delta_1,p_2+\delta_2) - W_2(p_1,p_2) - A_1(\delta_1) - A_2(\delta_2). \tag{9}$$

Here $A_i(x)=\tau b_i x d \sin\alpha_i$ $(i=1,2)$ is the work spent by the applied stress τ to expand the $\boldsymbol{b}_i$-loop, p_0 the parameter defining the initial positions of the segments ab and a′b′ immediately after the partial dislocation semiloop nucleation. Within the model, we assume that $p_0=1$ nm. Such a parameter is necessary to avoid the incorrectness of using the classical linear elasticity for describing the system right after the partial dislocation semiloop emission when a newly formed dislocation segment lies very close to the preexisting dislocation loop. The value 1 nm is also a standard estimate for the GB width in nanocrystalline metals.[29] Therefore it looks natural to put the initial position of the dislocation emitted from a GB at the distance 1 nm from it.

The following three-step algorithm was used to analyze the energy changes (6)–(9).

(1) First, the energy change ΔW_1^g given by Eq. (6) is calculated. If $\Delta W_1^g<0$ then generation of the first partial dislocation semiloop is energetically favorable for the given system, and we move to the next step. Otherwise, if $\Delta W_1^g\geqslant 0$, the generation of the partial dislocations is unfavorable.

(2) At the second step, it is assumed that the first partial dislocation semiloop already exists and its gliding segment ab is spaced by p_1 from the GB [Fig. 3(b)]. Two ways of the structure evolution are compared. Either the segment ab moves by a small fixed distance δ, or the second partial dislocation semiloop is nucleated. The energy changes $\Delta W_1^m(p_1,\delta)$ and $\Delta W_2^g(p_1)$ given by Eqs. (7) and (8), respectively, corresponding to these variants are calculated. If $\Delta W_2^g(p_1)<\Delta W_1^m(p_1,\delta)$ and $\Delta W_2^g(p_1)<0$ then generation of the second partial dislocation semiloop is supposed to occur, and we move to the next step of the algorithm. When $\Delta W_1^m(p_1,\delta)<\Delta W_2^g(p_1)$ and $\Delta W_1^m(p_1,\delta)<0$, it is energetically favorable for the segment ab to move to a new position $p_1+\delta$. Finally, if $\Delta W_1^m(p_1,\delta)\geqslant 0$ and $\Delta W_2^g(p_1)\geqslant 0$ then the system has reached its equilibrium state, and only one partial dislocation semiloop can exist for the given set of parameters.

(3) At the third step both the partial dislocation semiloops are supposed to exist, and their gliding segments ab and a′b′ are shifted by the distances p_1 and p_2, respectively, from the GB [Fig. 3(c)]. Here we find the equilibrium positions of these segments through the following iterative procedure. At each step of this procedure, the segments ab and a′b′ are assumed either staying immobile or moving forward or backward by a fixed distance δ. Besides the trivial situation where both segments do not move, there are eight possible ways for the system evolution which are characterized by the energy changes $\Delta W_2^m(p_1,\delta_1,p_2,\delta_2)$ given by Eq. (9). Here δ_1 and δ_2 can take on values from the set $-\delta$, 0, δ. Actually, with taking into account the restrictions on dislocation motion (gliding segments cannot leave the grain interior, the second segment cannot overtake the first one, etc.), the number of variants can be less than eight. At each step we compare the changes in the total energy of the system, corresponding to all possible displacements of the gliding segments ab and a′b′, and the parameters p_1 and p_2 receive the increments δ_1 and δ_2, corresponding to the minimal value $\Delta W_2^m(p_1,\delta_1,p_2,\delta_2)$ if that value is negative. The procedure is repeated until all values $\Delta W_2^m(p_1,\delta_1,p_2,\delta_2)$ become positive. This means that the system has reached the minimal value of its total energy and the current values of p_1 and p_2 are the equilibrium ones.

This algorithm can easily be implemented as a computer code which was done in this work in the MATHEMATICA 4.0 environment. For Al, the parameters[37] $G=26.5$ GPa, $\nu=0.345$, $a=0.404$ nm, and $\gamma=0.122$ J/m^2 were used. For easy comparing of our results with those obtained within the earlier models, we put $\beta=0$. Also we assumed that $r_c=b$, $r_{ci}=b_i$ $(i=1,2)$, and $\delta=0.01$ nm. Calculations were carried out for the grain size d in the range from 2 to 60 nm, the applied stress τ in the range from 0 to 2 GPa, and four values of the Burgers vector $\boldsymbol{b}$ of the preexistent dislocation loop: $\boldsymbol{b}=\boldsymbol{b}_0,1.2\boldsymbol{b}_0,1.4\boldsymbol{b}_0,1.6\boldsymbol{b}_0$. In both the gliding systems, the Burgers vectors $\boldsymbol{b}$, $\boldsymbol{b}_1$, $\boldsymbol{b}_2$ had the same magnitudes $b_0=a\sqrt{2}/2$ and $b_1=b_2=a\sqrt{6}/6$ but different orientations: in the 60°-I system $\alpha=30°$, $\alpha_1=0°$, and $\alpha_2=60°$; in the screw system $\alpha=90°$, $\alpha_1=60°$, and $\alpha_2=120°$. As a result, a data file containing the equilibrium positions of the segments ab and a′b′ was obtained for the given set of the system parameters.

IV. RESULTS OF MODEL

Of practical interest are the critical levels $\tau=\tau_{c1}$ and $\tau=\tau_{c2}$ at which generation of the first and second partial dislocation semiloops becomes energetically favorable, respectively. Strictly speaking, generation of a partial dislocation loop at a preexisting dislocation loop with the Burgers vector magnitude $b\geqslant b_0$ is always favorable.[47] However, after its generation, a newly formed partial dislocation semiloop may rest close to the GB that cannot be treated as "normal emission." That is why the critical stress is defined as a stress value at which the dislocation segment starts moving from its initial position $p_0=1$ nm. The dependences of τ_{c1} and τ_{c2} on

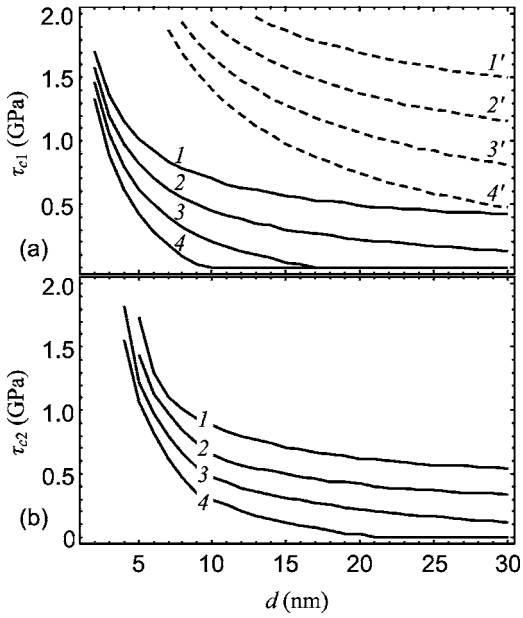

FIG. 4. Dependences of the critical stresses τ_{c1} (a) and τ_{c2} (b) on the grain size d for the 60°-I (solid lines) and screw (dashed line) gliding systems. Curves 1 and 1′ correspond to $\boldsymbol{b}=\boldsymbol{b}_0$, 2 and 2′ to $\boldsymbol{b}=1.2\boldsymbol{b}_0$, 3 and 3′ to $\boldsymbol{b}=1.4\boldsymbol{b}_0$, and 4 and 4′ to $\boldsymbol{b}=1.6\boldsymbol{b}_0$.

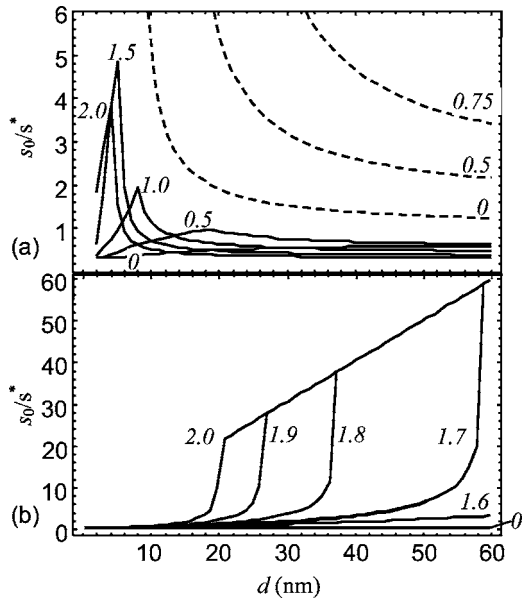

FIG. 5. The normalized SF width s_0/s^* via the grain size d for different levels of the stress τ (shown in GPa units at the curves): (a) 60°-I system and (b) screw system. The curves are calculated for $\boldsymbol{b}=\boldsymbol{b}_0$. The dashed curves show the results by Zhu *et al.* (Ref. 37).

the grain size d are shown in Figs. 4(a) and 4(b). The solid and dashed lines represent data for the 60°-I and screw gliding systems, respectively. As is seen, the generation of a partial dislocation semiloop belonging to the 60°-I system must occur easier compared to the screw system. Absence of the curves, corresponding to the screw system at Fig. 4(b) means that the second partial dislocation semiloop is not generated in this system. Also it is obvious from Fig. 4 that the higher the value of the Burgers vector $\boldsymbol{b}$ is, the easier the emission occurs. When $\boldsymbol{b}=\boldsymbol{b}_0$ (curves 1 and 1′), the critical values τ_{c1} and τ_{c2} are very high (>0.5 GPa). Such levels of stress cannot be reached even in nanocrystalline Al. But with the higher values of $\boldsymbol{b}$, the significant drop is observed for τ_{c1} and τ_{c2}, especially for the grain sizes $d>10$ nm. In the range of very small grain sizes (from 5 to 10 nm) the critical stresses are high even for $\boldsymbol{b}=1.6\boldsymbol{b}_0$ (curves 4, 4′), so the emission of partial dislocation semiloops should not occur in this case. This fact corresponds to the earlier results[12,32–34] that the generation of partial and split dislocations by GBs dominates over the other mechanisms when the grain size achieves some tens of nanometers.

We also analyzed the equilibrium SF width via d and τ. In this case, we did not consider the emission events. Instead, we created two partial dislocation semiloops at once and let the system relax to minimize its total energy. The SF width s_0 was calculated as $s_0=p_1-p_2$, where p_1 and p_2 are the equilibrium positions of the gliding segments ab and a′b′ [Fig. 3(c)]. Calculations were carried out for the value of Burgers vector of preexistent dislocation loop $\boldsymbol{b}=\boldsymbol{b}_0$. In Fig. 5, the ratio s_0/s^* in the 60°-I (a) and screw (b) gliding system is shown as a function of d for different values of τ. Here $s^*=Gb_1^2/[4\pi\gamma(1-\nu)]$ is the equilibrium SF width for a couple of straight partial dislocations in an infinite medium.[46] It is seen that wide SFs can be formed in both the gliding systems, however, in different ranges of d. In the 60°-I system, the SFs are wider at relatively small d, while in the screw system at larger d. In the screw system, the most important factor is the level of τ: when it is high enough ($\tau\approx 1.7-2$ GPa),the SFs can run across the whole grain [the linear branches of the curves in Fig. 5(b)].

The dashed curves in Fig. 5(a) represent the results by Zhu *et al.*[37] They are also similar to those of the earlier models.[9,36] One can see a drastic difference between the present and earlier results. The earlier models[9,36,37] predict anomalously wide SFs for nanocrystalline Al in the whole range of τ whereas our model gives this result for high τ only. Moreover, when $\tau=0$, our model gives even narrower SFs than those formed between straight dislocations in an infinite medium: $s_0/s^*<1$.

The main reason for such discrepancies (besides the incorrectness of energy calculations[9,36,37]) is that before it was assumed that the first emitted partial dislocation semiloop remains immobile during the second partial dislocation semiloop extension. The SF widening is then explained by the effect of the perfect lattice dislocation segments Aa′ and Bb′ [Fig. 3(c)]. The total energy minimization needs these segments to be shorter, even at the cost of lengthening the partial segments aa′ and bb′. As a result, an additional force appears which leads to SF widening. This would be true only if the first partial dislocation semiloop is prohibited to extend. Otherwise only an external stress τ could prevent the segments Aa′ and Bb′ from disappearing. If τ is low enough, they disappear, the second partial dislocation semiloop is localized near the GB, and the first partial dislocation semiloop will shrink to the second one under the common action of the SF and segments aa′ and bb′. Thus, again an additional force appears, but now it acts towards the SF contraction.

The results of our work fully confirm this reasoning. Under a low τ, nanocrystalline Al is expected to contain not

wide but narrow SFs compared to coarse-grained Al. The cause of anomalously wide SFs seems to be a high τ (>1 GPa), created in nanocrystalline Al at its nanoindentation[6] or production by severe deformation such as cryogenic ball milling.[7–9]

V. CONCLUDING REMARKS

In summary, we elaborated a 3D theoretical model describing the emission of partial dislocation semiloops from GBs accompanied by formation of SFs in fcc metals. The theory of dislocation loops was used to calculate the system energy more accurately compared to the earlier models.[9,36–39] By means of an original algorithm, we investigated both the generation of partial dislocation semiloops and dependence of the SF width on the grain size and applied stress level. The critical stress values for the partial dislocation semiloop generation were defined. It was found that emission of the partial dislocation semiloops belonging to the 60°-I gliding system is the most probable. We also showed that anomalously wide SFs in nanocrystalline Al are caused by high stresses but not by small grain size as was derived in the earlier models.[9,36–39] On the other hand, such high stresses are possible in nanocrystalline Al because the normal dislocation activity is suppressed by the small grain size. Therefore, although the small grain size is not directly connected with anomalously wide SFs in nanocrystalline Al, it represents the primary cause of this phenomenon.

ACKNOWLEDGMENTS

This work was supported, in part, by the Office of US Naval Research (Grant No. N00014-05-1-0217), INTAS (Grant No. 03-51-3779), INTAS-AIRBUS (Grant No. 04-80-7339), Russian Fund of Basic Research (Grant No. 04-01-00211), the Federal Agency of Science and Innovations (grant of the President of the Russian Federation MK-2902.2005.1), the Ministry of Education and Science of Russian Federation Program on Development of Scientific Potential of High School, Russian Academy of Sciences Program "Structural Mechanics of Materials and Construction Elements," and the St. Petersburg Scientific Center.

*Electronic address: ovidko@def.ipme.ru

[1] J. Schiøtz, T. Vegge, F. D. Di Tolla, and K. W. Jacobsen, Phys. Rev. B **60**, 11971 (1999).
[2] H. Van Swygenhoven, M. Spaczer, A. Caro, and D. Farkas, Phys. Rev. B **60**, 22 (1999).
[3] H. Van Swygenhoven and P. M. Derlet, Phys. Rev. B **64**, 224105 (2001).
[4] H. Van Swygenhoven, P. M. Derlet, and A. Hasnaoui, Phys. Rev. B **66**, 024101 (2002).
[5] H. Van Swygenhoven, P. M. Derlet, A. Hasnaoui, and M. Samaras, in *Nanostructures: Synthesis, Functional Properties and Applications*, edited by T. Tsakalakos, I. A. Ovid'ko, and A. K. Vasudevan (Kluwer, Dordrecht, 2003), p. 155.
[6] M. Chen, E. Ma, K. J. Hemker, H. Sheng, Y. M. Wang, and X. Cheng, Science **300**, 1275 (2003).
[7] X. Z. Liao, F. Zhou, E. J. Lavernia, S. G. Srinivasan, M. I. Baskes, D. W. He, and Y. T. Zhu, Appl. Phys. Lett. **83**, 632 (2003).
[8] X. Z. Liao, F. Zhou, E. J. Lavernia, D. W. He, and Y. T. Zhu, Appl. Phys. Lett. **83**, 5062 (2003).
[9] X. Z. Liao, S. G. Srinivasan, Y. H. Zhao, M. I. Baskes, Y. T. Zhu, F. Zhou, E. J. Lavernia, and H. F. Xu, Appl. Phys. Lett. **84**, 3564 (2004).
[10] S. V. Bobylev, M. Yu. Gutkin, and I. A. Ovid'ko, Acta Mater. **52**, 3793 (2004).
[11] A. G. Frozeth, P. M. Derlet, and H. Van Swygenhoven, Acta Mater. **52**, 5863 (2004).
[12] T. Shimokawa, A. Nakatani, and H. Kitagawa, Phys. Rev. B **71**, 224110 (2005).
[13] H. Yamaguchi, J. G. Belk, X. M. Zhang, J. L. Sudijono, M. R. Fahy, T. S. Jones, D. W. Pashley, and B. A. Joyce, Phys. Rev. B **55**, 1337 (1997).
[14] K. Thillman and A. Forster, Thin Solid Films **368**, 93 (2000).
[15] J. Zou, X. Z. Liao, D. J. H. Cockayne, and Z. M. Jiang, Appl. Phys. Lett. **81**, 1996 (2002).
[16] I. A. Ovid'ko, Phys. Rev. Lett. **88**, 046103 (2002).
[17] I. A. Ovid'ko and A. G. Sheinerman, Phys. Rev. B **66**, 245309 (2002).
[18] D. Halley, Y. Samson, A. Marty, P. Bayle-Guillemaud, C. Beigné, B. Gilles, and J. E. Mazille, Phys. Rev. B **65**, 205408 (2002).
[19] V. Fournée, J. Ledieu, T. Cai, and P. A. Thiel, Phys. Rev. B **67**, 155401 (2003).
[20] J. Kioseoglou, G. P. Dimitrakopulos, Ph. Komninou, H. M. Polatoglou, A. Serra, A. Béré, G. Nouet, and Th. Karakostas, Phys. Rev. B **70**, 115331 (2004).
[21] D. N. Zakharov, Z. Liliental-Weber, B. Wagner, Z. J. Reitmeier, E. A. Preble, and R. F. Davis, Phys. Rev. B **71**, 235334 (2005).
[22] I.-F. Tsu, S. E. Babcock, and D. L. Kaiser, J. Mater. Res. **11**, 1383 (1996).
[23] I.-F. Tsu, J.-L. Wang, D. L. Kaiser, and S. E. Babcock, Physica C **306**, 163 (1998).
[24] H. Kung, J. P. Hirth, S. R. Foltyn, P. N. Arendt, Q. X. Jia, and M. P. Maley, Philos. Mag. Lett. **81**, 85 (2001).
[25] M. Yu. Gutkin and I. A. Ovid'ko, Phys. Rev. B **63**, 064515 (2001).
[26] S. V. Bobylev and I. A. Ovid'ko, Phys. Rev. B **67**, 132506 (2003).
[27] Z. Zhang, W. Sigle, W. Kurtz, and M. Rühle, Phys. Rev. B **66**, 214112 (2002).
[28] K. S. Kumar, H. Van Swygenhoven, and S. Suresh, Acta Mater. **51**, 5743 (2003).
[29] M. Yu. Gutkin and I. A. Ovid'ko, *Plastic Deformation in Nanocrystalline Materials* (Springer, Berlin, 2004).
[30] I. A. Ovid'ko, Int. Mater. Rev. **50**, 65 (2005).
[31] B. Q. Han, E. Lavernia, and F. A. Mohamed, Rev. Adv. Mater. Sci. **9**, 1 (2005).
[32] V. Yamakov, D. Wolf, M. Salazar, S. R. Phillpot, and H. Gleiter, Acta Mater. **49**, 2713 (2001).

[33] V. Yamakov, D. Wolf, S. R. Phillpot, A. K. Mukherjee, and H. Gleiter, Nat. Mater. **1**, 45 (2002).
[34] P. M. Derlet and H. Van Swygenhoven, Scr. Mater. **47**, 719 (2002).
[35] H. J. Frost and M. S. Ashby, *Deformation-Mechanism Maps* (Pergamon Press, Oxford, 1982).
[36] S. V. Bobylev and I. A. Ovid'ko, Rev. Adv. Mater. Sci. **7**, 75 (2004).
[37] Y. T. Zhu, X. Z. Liao, S. G. Srinivasan, Y. H. Zha, M. I. Baskes, F. Zhou, and E. J. Lavernia, Appl. Phys. Lett. **85**, 5049 (2004).
[38] Y. T. Zhu, X. Z. Liao, S. G. Srinivasan, and E. J. Lavernia, J. Appl. Phys. **98**, 034319 (2005).
[39] R. J. Asaro and S. Suresh, Acta Mater. **53**, 3369 (2005).
[40] A. P. Sutton and R. W. Balluffi, *Interfaces in Crystalline Materials* (Oxford Science Publications, Oxford, 1996).
[41] K. A. Padmanabhan and H. Gleiter, Mater. Sci. Eng., A **381**, 28 (2004).
[42] A. S. Argon, Acta Mater. **27**, 47 (1979).
[43] M. Yu. Gutkin and A. G. Sheinerman, Phys. Status Solidi B **241**, 1810 (2004).
[44] T. Mura, *Micromechanics of Defects in Solids* (Martinus Nijhoff, Dordrecht, 1987).
[45] M. Yu. Gutkin, I. A. Ovid'ko, and Yu. I. Meshcheryakov, J. Phys. III **3**, 1563 (1993).
[46] J. P. Hirth and J. Lothe, *Theory of Dislocations* (Wiley, New York, 1982).
[47] M. Yu. Gutkin and I. A. Ovid'ko, Philos. Mag. (to be published).